ELSEVIER

International Journal of Solids and Structures 41 (2004) 459–480

INTERNATIONAL JOURNAL OF SOLIDS and STRUCTURES

www.elsevier.com/locate/ijsolstr

On the transmission of transient elastodynamic waves at a frictionless contact interface; application to a weakly coupled bimaterial

Quentin Grimal *, Salah Naïli *, Alexandre Watzky

Laboratoire de Mécanique Physique, CNRS UMR 7052 B2OA, Faculté des Sciences et Technologie, Université Paris XII-Val de Marne, 61, Avenue du Général de Gaulle, 94010 Creteil Cédex, France

Received 1 January 2003; received in revised form 2 June 2003

Abstract

A method is presented for a detailed quantitative analysis of the elastic waves interaction with a frictionless sliding interface between two linearly elastic, isotropic and homogeneous half-spaces (media 1 and 2). Frictionless contact (zero shear stresses and discontinuity of tangential displacements at the interface) is relevant, for instance, when media are separated by a thin fluid layer. The required transmission/reflection coefficients of plane waves at the interface are derived in closed form. The elastodynamic problem consists in calculating exact time domain Green's functions (for displacements and stresses) in medium 2, when a point force acts inside medium 1. They are obtained in two steps: (1) the generalized ray theory yields solutions in a Laplace–Fourier transform domain for each transmitted wave (*PP*, *PS*, *SP* and *SS*); (2) the Cagniard–de Hoop method is used to return in the time-space domain. Numerical results are relevant to the propagation of an impact wave in an idealized model of the thorax; media 1 and 2 represent the thoracic wall (''stiff'') and the lung (''compliant''). The wave field transmitted at the frictionless interface is compared to that transmitted at a welded interface. It is found that (i) *S*-waves amplitudes are negligible; (ii) the *P*-wave field is only slightly changed; (iii) these effects are characteristic of the weak acoustic coupling.

Keywords: Frictionless contact; Wave; Interface; Reflection and transmission coefficients; Generalized rays; Cagniard–de Hoop

1. Introduction

The work presented in this paper is an analysis of the transmission of elastic waves at the interface between two solids in frictionless sliding contact, i.e., zero shear stresses and discontinuity of tangential displacements are assumed at the interface. This contact condition is relevant to model an interface between two media which allow for negligible friction assumption; for instance, two media separated by a thin fluid layer, but which are bonded in such a way that no void can be created at the interface. The motivation of

* Corresponding authors. Tel.: +33-1-45-17-14-45/15-72; fax: +33-1-45-17-14-33.
E-mail addresses: grimal@univ-paris12.fr (Q. Grimal), naili@univ-paris12.fr (S. Naïli), watzky@univ-paris12.fr (A. Watzky).

0020-7683/$ - see front matter © 2003 Elsevier Ltd. All rights reserved.
doi:10.1016/j.ijsolstr.2003.09.025

the present study is to characterize the propagation of acoustic waves in the human thorax; and, in particular, their transmission at the interface between the thoracic wall and the lung. The lung and the thoracic wall are separated by a small potential space—the pleural cavity—which contains a lubricating fluid allowing the media to move easily on each other; in addition, under normal physiological conditions, pressure in the cavity is below atmospheric pressure so that the media remain in contact. Hence frictionless sliding may be assumed at the thoracic wall-lung interface. The frictionless contact condition may as well be relevant to model cracks and lubricated contacts, and it may be considered in preliminary studies previous to elaborated models of contact with friction.

The acoustic response of solids in *welded* contact (continuity of displacements and normal stresses) and at a fluid/solid interface have been extensively studied; in particular, the associated transmission/reflection coefficients are easily found in the literature (see Aki and Richard, 1980; Brekhovskikh, 1980). In contrast, *frictionless sliding* contact has seldom been considered; some related works were conducted by Achenbach and Epstein (1967) who investigated the propagation of interface waves and, more recently, by Shuvalov and Gorkunova (1999) who considered the transmission/reflection of plane waves between anisotropic media.

Qualitative knowledge on the transmission of elastic waves at an interface may in some cases be inferred straightforward from a simple study of plane waves. However such an analysis is restricted to those cases where the source of waves and the receiver of interest are both "far" enough from the interface (which is equivalent to a "high" frequencies hypothesis).

In the present paper, a method is presented for a detailed quantitative analysis of the interaction of elastic waves with a frictionless interface. The generalized ray (GR)/Cagniard–de Hoop method which has been extensively used with welded contact interface is exploited; the main benefit of using this method is to work with an exact solution of the elastodynamic problem.

When dealing with analytical methods of solution, plane or spherical waves are considered depending on the distance of the interface from the source. Regarding the transmission of elastic waves at a plane interface, spherical and plane waves problems are, in essence, managed the same way: the amplitudes of incident plane waves are multiplied by transmission coefficients that are functions of the incidence of the waves; spherical waves are split into an infinite sum of plane waves of various incidences, each multiplied by a transmission coefficient—in this case the coefficients are called "generalized coefficients" (Spencer, 1960), but they are the same. The generalized ray theory (Pao and Gajewski, 1977; Aki and Richard, 1980) used in this study, which was developed for the analysis of wave fields generated by finite-size and time-dependant sources, heavily relies on the generalized transmission/reflection coefficients.

For the purposes of the study, we have derived the transmission/reflection coefficients at the frictionless interface; although their derivation does not involve formal difficulties, the coefficients presented in this paper could not be found in the literature dedicated to wave propagation. We give both the closed form analytical formula for each coefficient and a procedure that yields the coefficients after the numerical inversion of a matrix.

In this study the wave field incident at the interface consists in longitudinal and transverse waves generated by an impulsive point force at a finite distance from the interface. The media on each side of the interface are semi-infinite elastic solids. The force is buried in one of the media. The solution for each displacement or component of the stress tensor consists in a sum of contributions due to transverse and longitudinal waves; each contribution is obtained under the form of a convolution product between the history of the applied force and an exact Green's function of the elastodynamics problem. These solutions are arrived at in two steps: (1) by means of integral transformations, the solution is obtained in a Laplace–Fourier transform domain with the help of the generalized ray theory; (2) then an inverse transformation procedure—Cagniard–de Hoop (CdH) method (Cagniard, 1962; de Hoop, 1960)—is applied to return in the time-space domain. Application of the CdH method involves an integration along a contour in the complex slowness plane which has required a detailed mathematical analysis of the occurrence of poles of

the transmission/reflection coefficients. Solutions thus obtained are *exact*, that is, they are valid whatever the frequency content of the applied impulse and the distances from the interface.

Concerning the mechanical properties of the media, we focus on the special case where medium 1—in which the source is located—is "stiff" in comparison to medium 2. This corresponds to the biological structure mentioned above where the media respectively represent the thoracic wall and the lung. The lung is an organ which can easily be damaged by the propagation of an impact wave generated by a "high-velocity" non-penetrating impact on the thorax (Fung, 1990; Grimal et al., 2002c). The respective role of longitudinal and transverse waves in the mechanism of injury of the lung are not clear. As these roles can hardly be elucidated by means of experiments on living tissues, modeling the wave phenomena is essential; a better knowledge of wave propagation patterns should help identify the phenomena involved in the mechanisms of lung injury. The transmission of elastic waves in an idealized model of the thorax identical to the one considered in the present study but with a welded interface has already been investigated, with similar methods of solutions, in Grimal et al. (2002a) (plane interface) and Grimal et al. (2002b) (spherical interface). (In Grimal et al. (2002a,b), we used the adjectives "hard" and "soft"; since they can be misleading we use in the present paper "stiff" and "compliant" instead.) The specific motivation for the present work is to quantify the influence of the contact condition, assumed at the interface between the thoracic wall and the lung, on the repartition of energy in the medium representing the lung.

Numerical results basically are a comparison of the transmitted wave fields for welded and frictionless contact. The selection of the results presented has been motivated by two aims: (i) illustrate the use of the CdH method to characterize a transmitted wave field at an interface with given contact conditions; (ii) elucidate the nature of the wave field in the lung when a transient pulse is propagated in a model of the thorax. The quantitative results obtained are consistent with the qualitative behavior that can be inferred from the values of the plane wave transmission coefficients. It is to note that the numerical results presented are not only of interest for the biomechanical problem considered but also for any problem of wave propagation in weakly coupled structures.

The present paper is organized as follows: after this introduction as background, Section 2 gives a description of the configuration and a formulation of the basic elastodynamic equations. In Section 3 we show how the transform domain counterparts of the space-time domain quantities are obtained by means of a temporal Laplace transformation and a two-dimensional spatial Fourier transformation; then the transform domain wave propagation problem is solved formally with the help of the GR theory. The transmission coefficients at the frictionless interface that appear in the formal solution obtained in Section 3 are derived in Section 4; although the derivation technique is standard, some details are given so that the calculations can easily be reproduced. In Section 5, the transformation back to the space-time domain with the CdH method is presented. This section includes a discussion of the analyticity of the transform domain solution, which is capital in the CdH method; the discussion of the occurrence of poles in the complex slowness plane due to the transmission coefficients at the frictionless interface is given in the Appendix A. Section 6 is dedicated to numerical results. Finally, a discussion of the potential use of the work in understanding lung injury due to impact loading, and the conclusions of the analysis, are presented Section 7.

2. Description of the configuration and formulation of the problem

2.1. Configuration and definitions

The model configuration (Fig. 1) consists of two half-spaces—media 1 and 2—in contact at a plane interface. The position is specified through the coordinates (x_1, x_2, x_3) with respect to a Cartesian reference frame $R(\mathrm{O}; \mathbf{x}_1, \mathbf{x}_2, \mathbf{x}_3)$ where O is the origin and $(\mathbf{x}_1, \mathbf{x}_2, \mathbf{x}_3)$ is an orthonormal basis for the space; the $\mathbf{x}_3$-axis is taken perpendicular to the interface. Each layer is homogeneous, isotropic and obeys Hooke's law; for

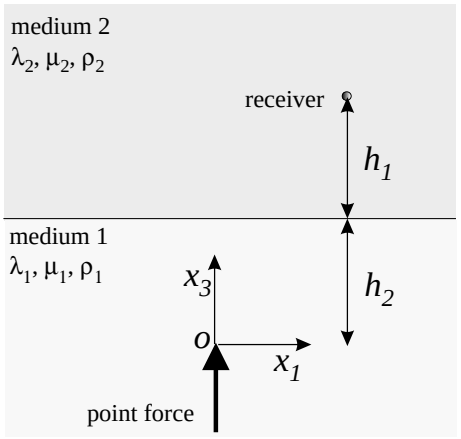

Fig. 1. Configuration and coordinate system.

the characterization of the elastic properties, the Lamé constants λ and μ are used, and the mass density is denoted by ρ. The elastic wave motion will be characterized in R by the components σ_{ij} of the Cauchy stress tensor and by the components v_i of the particle velocity $\mathbf{v}$. At the interface, located at $x_3 = x_I$, we will consider alternatively welded and frictionless sliding contact.

The source that generates the wave motion is a point force, of direction $\mathbf{x}_3$, buried in medium 1; without loss of generality, we assume that the source is located at the origin O of the reference frame. The initial condition is that all the layers are at rest for $t \leqslant 0$.

Due to the nature of the source considered and to the geometrical configuration, both longitudinal (pressure) waves and transverse (shear) waves with vertical polarization will propagate. Pressure and shear waves are denoted P- and S-waves respectively; letters P and S are used for quantities relative to P- and S-waves, respectively. Wave speeds are defined by $c_P = \sqrt{(\lambda + 2\mu)/\rho}$ and $c_S = \sqrt{\mu/\rho}$, and waves slownesses by $s_{P,S} = 1/c_{P,S}$. All through the paper, each time a comma appears between P and S means that the quantities relative to P- or S-waves respectively must be used. Shear waves with horizontal polarization are associated with the notation SH. Note that we somewhat simplify the problem as we consider a point force of direction $\mathbf{x}_3$ which do not generates SH-waves (however, the expressions of the transmission coefficients obtained in Section 4 for all the possible polarizations show that SH-waves are not transmitted in medium 2).

Throughout this paper, superscripts (1) and (2) will refer to media 1 and 2, respectively; however, superscripts may be omitted in equations valid for both media, if no ambiguity results.

2.2. Governing equations, boundary and initial conditions

The equation of motion is

$$\partial_j \sigma_{ij} - \rho \partial_t v_i = -f_0 \phi(t) \delta(x_1, x_2, x_3) \delta_{i3}, \quad i, j = 1, 2, 3, \tag{1}$$

where ∂_j and ∂_t denote partial derivatives with respect to x_j and to time respectively, δ_{ij} is the Kronecker symbol and Einstein summation convention is used. The right-hand side term of Eq. (1) stands for the buried point force: $\phi(t)$ describes the history of the source (with $\phi(t) = 0$ for $t < 0$), f_0 is the source strength and $\delta(x_1, x_2, x_3)$ is the three-dimensional Dirac function. The time derivative of Hooke's constitutive law for an elastic isotropic medium is introduced as

$$\partial_t \sigma_{ij} - \lambda \delta_{ij} \delta_{pq} \partial_q v_p - \mu(\partial_i v_j + \partial_j v_i) = 0. \tag{2}$$

Frictionless sliding interface. If frictionless contact (also sometimes referred to as "smooth contact") is assumed, the boundary conditions at the interface (plane $x_3 = x_I$) are

$$\begin{aligned} &[\![v_3]\!] = 0, \quad [\![\sigma_{33}]\!] = 0, \\ &\sigma_{13}^{(1)}(x_1, x_2, x_I, t) = \sigma_{23}^{(1)}(x_1, x_2, x_I, t) = 0, \\ &\sigma_{13}^{(2)}(x_1, x_2, x_I, t) = \sigma_{23}^{(2)}(x_1, x_2, x_I, t) = 0, \end{aligned} \tag{3}$$

where $[\![\cdot]\!]$ denotes the jump of a quantity across the interface.

Welded interface. If welded contact is assumed, the boundary conditions at the interface are

$$[\![\sigma_{13}]\!] = [\![\sigma_{23}]\!] = [\![\sigma_{33}]\!] = 0 \quad \text{and} \quad [\![v_1]\!] = [\![v_2]\!] = [\![v_3]\!] = 0. \tag{4}$$

3. Solution in the transform-domain

Taking into account the time invariance of the configuration, we subject the equations given in Section 2.2 to a one-sided Laplace transform with respect to time. As an example, the space-time domain particle velocity $v_i(\mathbf{x}, t)$ is transformed to its space-Laplace domain counterpart $\hat{v}_i(\mathbf{x}, p)$ according to

$$\hat{v}_j(\mathbf{x}, p) = \int_0^\infty \exp(-pt) v_j(\mathbf{x}, t)\, \mathrm{d}t,$$

where p is real and positive. Subsequently, the shift invariance of the configuration with respect to x_1 and x_2 is exploited by applying a two-dimensional Fourier transformation to the Laplace-transformed equations. The Fourier-Laplace domain counterpart or, shortly, the transform domain counterpart $\tilde{v}_j(k_1, k_2, x_3, p)$ of $\hat{v}_j(\mathbf{x}, p)$ is

$$\tilde{v}_j(k_1, k_2, x_3, p) = \int_{-\infty}^\infty \int_{-\infty}^\infty \exp[\mathrm{i}p(k_1 x_1 + k_2 x_2)] \hat{v}_j \, \mathrm{d}x_1 \, \mathrm{d}x_2,$$

where pk_1 and pk_2 are the—real—Fourier transform parameters. The inverse Fourier transformation is

$$\hat{v}_j(\mathbf{x}, p) = (p/2\pi)^2 \int_{-\infty}^\infty \int_{-\infty}^\infty \exp[-\mathrm{i}p(k_1 x_1 + k_2 x_2)] \tilde{v}_j \, \mathrm{d}k_1 \, \mathrm{d}k_2.$$

After elimination, in the transform domain counterparts of Eqs. (1) and (2), of the stress components that may show a jump discontinuity across the interface, six transform domain unknown state quantities remain for representing the wave field in each medium; they are arranged into the "motion-stress" state vector $\tilde{\mathbf{b}} = (\tilde{v}_1, \tilde{v}_2, \tilde{v}_3, -\tilde{\sigma}_{13}, -\tilde{\sigma}_{23}, -\tilde{\sigma}_{33})^{\mathrm{T}}$ (here T means transpose). In both media, the differential equation for $\tilde{\mathbf{b}}$ takes the form (see van der Hijden (1987) for details)

$$\partial_3 \tilde{\mathbf{b}} = -pA\tilde{\mathbf{b}} + \hat{\phi}(p)\mathbf{X}\delta(x_3), \tag{5}$$

where $\hat{\phi}(p)\mathbf{X}\delta(x_3)$ is the transform domain source vector, $\hat{\phi}(p)$ is the Laplace transform of $\phi(t)$ and A is a 6×6 matrix; note that the source vector is zero for medium 2 which is free of source. Instead of solving directly Eq. (5), it is convenient to introduce the linear transformation

$$\tilde{\mathbf{b}} = D\mathbf{w}, \tag{6}$$

where the six components of $\mathbf{w}$—called the "wave vector"—stand for six independent wave motions identified below. Each column of matrix D is an eigenvector of matrix A (van der Hijden, 1987, p. 53):

$$D = \begin{pmatrix} c_P \mathrm{i}k_1 & \mathrm{i}c_S s_3^S k_1 S^{-1} & -\mathrm{i}k_2 S^{-1} & c_P \mathrm{i}k_1 & -\mathrm{i}c_S s_3^S k_1 S^{-1} & -\mathrm{i}k_2 S^{-1} \\ c_P \mathrm{i}k_2 & \mathrm{i}c_S s_3^S k_2 S^{-1} & \mathrm{i}k_1 S^{-1} & c_P \mathrm{i}k_2 & -\mathrm{i}c_S s_3^S k_2 S^{-1} & \mathrm{i}k_1 S^{-1} \\ -c_P s_3^P & c_S S & 0 & c_P s_3^P & c_S S & 0 \\ -2\mu c_P s_3^P \mathrm{i}k_1 & -2\mathrm{i}\mu c_S \chi k_1 S^{-1} & \mu \mathrm{i} s_3^S k_2 S^{-1} & 2\mu c_P s_3^P \mathrm{i}k_1 & -2\mu \mathrm{i} c_S \chi k_1 S^{-1} & -\mu \mathrm{i} s_3^S k_2 S^{-1} \\ -2\mu c_P s_3^P \mathrm{i}k_2 & -2\mathrm{i}\mu c_S \chi k_2 S^{-1} & -\mu \mathrm{i} s_3^S k_1 S^{-1} & 2\mu c_P s_3^P \mathrm{i}k_2 & -2\mu \mathrm{i} c_S \chi k_2 S^{-1} & \mu \mathrm{i} s_3^S k_1 S^{-1} \\ 2\mu c_P \chi & -2\mu S c_S s_3^S & 0 & 2\mu c_P \chi & 2\mu S c_S s_3^S & 0 \end{pmatrix},$$

where $S^2 = -(k_1^2 + k_2^2)$, $\chi = 0.5 s_S^2 - S^2$ and $s_3^{P,S} = (s_{P,S}^2 - S^2)^{1/2}$. Due to the normalization of D, w_1, w_2 and w_3 represent, respectively, the particle velocities associated with P-waves, S-waves and SH-waves propagating in the direction of decreasing $\mathbf{x}_3$; w_4, w_5 and w_6 are their counterparts in the direction of increasing $\mathbf{x}_3$. Substituting Eq. (6) into Eq. (5) yields the following differential equation for the wave vector

$$\partial_3 \mathbf{w} = -p \Lambda \mathbf{w} + \hat{\phi}(p) D^{-1} \mathbf{X} \delta(x_3), \tag{7}$$

where Λ is a diagonal matrix whose non-zero terms are the eigenvalues of A

$$\Lambda_{11} = -s_3^P, \quad \Lambda_{22} = -s_3^S, \quad \Lambda_{33} = -s_3^S, \quad \Lambda_{44} = s_3^P, \quad \Lambda_{55} = s_3^S, \quad \Lambda_{66} = s_3^S.$$

In the case of interest for the present study, the non-zero wave vector components of the wave field incident at the interface in medium 1 are the two following solutions of Eq. (7)

$$\begin{aligned} w_4^{(1)} &= \hat{\phi}(p) W_4 \times \exp[-p s_3^{P;1} x_3], \\ w_5^{(1)} &= \hat{\phi}(p) W_5 \times \exp[-p s_3^{S;1} x_3], \end{aligned} \tag{8}$$

which have the structure of waves propagating along $\mathbf{x_3}$. The amplitude factors $W_n = \sum_{k=1}^{6} \{D_{nk}^{-1} X_k\}$ are obtained from the boundary conditions at the source in medium 1 (van der Hijden, 1987, p. 57)

$$W_4 = \frac{f_0 c_{P;1}}{2(\lambda_1 + 2\mu_1)}, \quad W_5 = \frac{f_0 c_{S;1} S}{2 s_3^{S;1} \mu_1}. \tag{9}$$

The expressions for the transmitted wave field $(w_4^{(2)}, w_5^{(2)})$ and for the reflected wave field $(w_1^{(1)}, w_2^{(1)})$ assume a form similar to Eqs. (8). The amplitude factors for these wave fields follow upon multiplication of the amplitudes of the incident waves with relevant transmission/reflection coefficients; this is, in essence, the foundation of the generalized ray theory (Spencer, 1960; Pao and Gajewski, 1977). From now on, we focus on the transmitted wave field. Phase terms appearing in the exponential functions in Eqs. (8) must be modified so that the whole propagation path is described. Let h_1 and h_2 be the distances travelled by the waves, from the source to the receiver, along x_3 (see Fig. 1), and let α and β denote the polarizations (P or S) in media 1 and 2, respectively. The Laplace transformed state vector in medium 2, corresponding to the transmitted wave field, may be formally written as

$$\hat{b}_j^{(2)}(\mathbf{x}, p) = \hat{b}_j^{P \to P}(\mathbf{x}, p) + \hat{b}_j^{P \to S}(\mathbf{x}, p) + \hat{b}_j^{S \to P}(\mathbf{x}, p) + \hat{b}_j^{S \to S}(\mathbf{x}, p),$$

where each $\hat{\mathbf{b}}^{\alpha \to \beta}$ represents the contribution of a GR (a particular wave). Each GR is given by

$$\hat{b}_j^{\alpha \to \beta}(\mathbf{x}, p) = \hat{\phi}(p) \left(\frac{p}{2\pi} \right)^2 \int_{-\infty}^{\infty} \int_{-\infty}^{\infty} B_j^{\alpha \to \beta}(k_1, k_2) T_{\alpha \to \beta} \exp[-p(\mathrm{i}k_1 x_1 + \mathrm{i}k_2 x_2 + s_3^{\alpha;1} h_1 + s_3^{\beta;2} h_2)] \, \mathrm{d}k_1 \, \mathrm{d}k_2 \tag{10}$$

with

$$B_i^{\alpha \to \beta}(k_1, k_2) = D_{im}^{(2)} W_l^{(1)},$$

where subscripts l and m are associated with polarizations α and β, respectively (in the present paper, l and m take the values 4 or 5 depending on the GR under study; for example, the ray denoted by $P \to S$ is

associated with $l = 4$ and $m = 5$). We have denoted by $T_{\alpha\to\beta}$ the transmission coefficient corresponding to the GR $\hat{\mathbf{b}}^{\alpha\to\beta}$.

The terms $T_{\alpha\to\beta}$ may be taken to be transmission coefficients at a *frictionless* or a *welded* interface, alternatively. For the welded contact condition, the closed-form expressions of plane waves coefficients, as given by Aki and Richard (1980, p. 144), have been used (the coefficient were also reproduced in Grimal et al. (2002a)). For the frictionless contact conditions, the coefficients are derived in the next section.

4. Derivation of the transmission/reflection coefficients for the frictionless interface

For the purposes of the present study, the transmission coefficients of plane waves at a frictionless interface are required. These coefficients could not be found in the literature (note that most of the standard textbooks deal with welded contact) and are derived in this section. The method of derivation uses the formalism employed in the previous section but is, in essence, a standard procedure. Only the four transmission coefficients for *P*- and *S*-waves, from medium 1 to medium 2, are needed for the present study; however, for the sake of completeness, the derivation of all the twenty transmission/reflection coefficients is presented.

Each component of the wave vector $\mathbf{w}$ represents the amplitude of a wave specified both by a polarization and a direction of propagation with respect to x_3. It is convenient to split $\mathbf{w}$ in two parts:

$$\mathbf{w} = (\mathbf{w}^-, \mathbf{w}^+), \quad \text{with } \mathbf{w}^- = (w_1, w_2, w_3) \quad \text{and} \quad \mathbf{w}^+ = (w_4, w_5, w_6), \tag{11}$$

where the components associated with downgoing (decreasing x_3) and upgoing waves (increasing x_3) are indicated by (−) and (+), respectively. In what follows, we shall split other quantities in the same manner and use the same sign convention. Vectors $\mathbf{w}^-$ and $\mathbf{w}^+$ each have three components $(w_1^\pm, w_2^\pm, w_3^\pm)$ corresponding to *P*-, *S*- and *SH*-waves, respectively.

We apply the scattering matrix formalism (Aki and Richard, 1980, p. 144), illustrated in Fig. 2, at the interface between media 1 and 2: the amplitudes of the waves propagating away from the interface ($\mathbf{w}^{(1)-}$ and $\mathbf{w}^{(2)+}$) are expressed in terms of the waves propagating towards the interface ($\mathbf{w}^{(1)+}$ and $\mathbf{w}^{(2)-}$)

$$\begin{aligned} \mathbf{w}^{(1)-} &= R^+\mathbf{w}^{(1)+} + T^-\mathbf{w}^{(2)-}, \\ \mathbf{w}^{(2)+} &= T^+\mathbf{w}^{(1)+} + R^-\mathbf{w}^{(2)-}, \end{aligned} \tag{12}$$

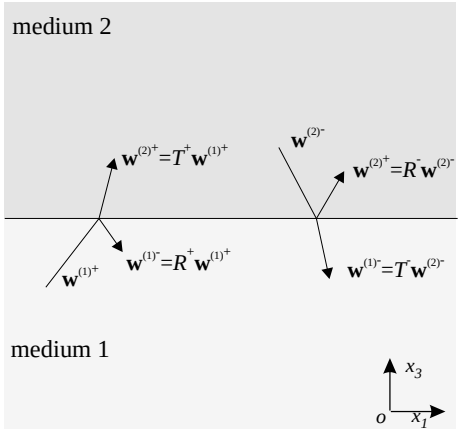

Fig. 2. Illustration of the scattering matrix formalism.

where $T^{\pm}$ and $R^{\pm}$ are 3×3 transmission and reflection coefficients matrices (note that the superscripts of T and R correspond to the direction of propagation of the incident waves) that assume the following form

$$R^{\pm} = \begin{pmatrix} R^{\pm}_{P\to P} & R^{\pm}_{S\to P} & 0 \\ R^{\pm}_{P\to S} & R^{\pm}_{S\to S} & 0 \\ 0 & 0 & R^{\pm}_{SH\to SH} \end{pmatrix} \quad T^{\pm} = \begin{pmatrix} T^{\pm}_{P\to P} & T^{\pm}_{S\to P} & 0 \\ T^{\pm}_{P\to S} & T^{\pm}_{S\to S} & 0 \\ 0 & 0 & T^{\pm}_{SH\to SH} \end{pmatrix}, \tag{13}$$

where the combinations of subscripts P and S hold for the respective mode conversion or conservation; for instance, $T^{+}_{S\to P}$ is the transmission coefficient associated with an upgoing incident S-wave in medium 1, transmitted in medium 2 as a P-wave. Coefficients corresponding to coupling between P- or S-, and SH-waves, are zero since motion in planes parallel to the interface is decoupled from the motion in planes perpendicular to the interface. Hence the problem of finding the four coefficients corresponding to SH-wave motion is decoupled from the problem of finding the other 16 coefficients.

The contact conditions at the frictionless interface given by Eqs. (3) are rewritten, in the transform-domain, in terms of the wave vector components (see Eq. (6))

$$\begin{aligned} &\sum_{n=1}^{6} D^{(1)}_{3n} w^{(1)}_n = \sum_{n=1}^{6} D^{(2)}_{3n} w^{(2)}_n, \quad \sum_{n=1}^{6} D^{(1)}_{4n} w^{(1)}_n = 0, \quad \sum_{n=1}^{6} D^{(2)}_{4n} w^{(2)}_n = 0, \\ &\sum_{n=1}^{6} D^{(1)}_{6n} w^{(1)}_n = \sum_{n=1}^{6} D^{(2)}_{6n} w^{(2)}_n, \quad \sum_{n=1}^{6} D^{(1)}_{5n} w^{(1)}_n = 0, \quad \sum_{n=1}^{6} D^{(2)}_{5n} w^{(2)}_n = 0. \end{aligned} \tag{14}$$

For notational simplicity we introduce $\mathbf{D}_k$ as the vector corresponding to the kth line of matrix D. It can be split in two parts associated with upgoing and downgoing waves as

$$\mathbf{D}_k = (\mathbf{D}^{-}_k, \mathbf{D}^{+}_k).$$

Introducing Eqs. (12) in Eqs. (14), a system of equations where the transmission/reflection coefficients appear is obtained

$$\begin{aligned} &\mathbf{D}^{(1)-}_3 (R^{+}\mathbf{w}^{(1)+} + T^{-}\mathbf{w}^{(2)-}) + \mathbf{D}^{(1)+}_3 \mathbf{w}^{(1)+} = \mathbf{D}^{(2)-}_3 \mathbf{w}^{(2)-} + \mathbf{D}^{(2)+}_3 (T^{+}\mathbf{w}^{(1)+} + R^{-}\mathbf{w}^{(2)-}), \\ &\mathbf{D}^{(1)-}_6 (R^{+}\mathbf{w}^{(1)+} + T^{-}\mathbf{w}^{(2)-}) + \mathbf{D}^{(1)+}_6 \mathbf{w}^{(1)+} = \mathbf{D}^{(2)-}_6 \mathbf{w}^{(2)-} + \mathbf{D}^{(2)+}_6 (T^{+}\mathbf{w}^{(1)+} + R^{-}\mathbf{w}^{(2)-}), \\ &\mathbf{D}^{(1)-}_4 (R^{+}\mathbf{w}^{(1)+} + T^{-}\mathbf{w}^{(2)-}) + \mathbf{D}^{(1)+}_4 \mathbf{w}^{(1)+} = 0, \\ &\mathbf{D}^{(1)-}_5 (R^{+}\mathbf{w}^{(1)+} + T^{-}\mathbf{w}^{(2)-}) + \mathbf{D}^{(1)+}_5 \mathbf{w}^{(1)+} = 0, \\ &\mathbf{D}^{(2)-}_4 \mathbf{w}^{(2)-} + \mathbf{D}^{(2)+}_4 (T^{+}\mathbf{w}^{(1)+} + R^{-}\mathbf{w}^{(2)-}) = 0, \\ &\mathbf{D}^{(2)-}_5 \mathbf{w}^{(2)-} + \mathbf{D}^{(2)+}_5 (T^{+}\mathbf{w}^{(1)+} + R^{-}\mathbf{w}^{(2)-}) = 0. \end{aligned} \tag{15}$$

Eqs. (15) are valid for any incident wave amplitude, that is, for any value of $w^{(1)+}_1$, $w^{(1)+}_2$, $w^{(1)+}_3$, $w^{(2)-}_1$, $w^{(2)-}_2$ and $w^{(2)-}_3$. Upon setting $w^{(1)+}_1 = w^{(1)+}_2 = w^{(2)-}_1 = w^{(2)-}_2 = 0$ and by using the form of the coefficient matrices given by Eqs. (13), it can be shown straight forward that the transmission and reflection coefficients for SH-waves at the frictionless interface are

$$T^{\pm}_{SH\to SH} = 0; \quad R^{\pm}_{SH\to SH} = 1.$$

These values correspond to transmission and reflection of SH-waves at a free surface.

The coefficients associated with P- and S-waves are derived by setting $w_3^{(1)+} = w_3^{(2)-} = 0$, so that Eqs. (15) is rewritten as a system of four equations only—Eqs. $(15)_3$ and $(15)_4$ on the one hand, and Eqs. $(15)_5$ and $(15)_6$ on the other hand, are found to be equivalent. Then, by taking in Eqs. (15) successively zero for three of the four amplitudes $w_1^{(1)+}$, $w_2^{(1)+}$, $w_1^{(2)-}$ and $w_2^{(2)-}$, *four* systems of four linear equations are derived; each of these systems yields four transmission/reflection coefficients. Written in the matrix form $M\mathbf{a} = \mathbf{y}$, the four systems have the same matrix M. Defining by Y the 4×4 matrix whose columns are the right-hand-side vectors $\mathbf{y}$ obtained for each system, the coefficients for P- and S-waves are given by

$$\begin{pmatrix} R'^{+} & T'^{-} \\ T'^{+} & R'^{-} \end{pmatrix} = M^{-1}Y, \tag{16}$$

where $R'^{\pm}$ and $T'^{\pm}$ are 2×2 matrices built with the P/S parts of matrices $R^{\pm}$ and $T^{\pm}$ in Eqs. (13). Matrices Y and M are respectively

$$Y = \begin{pmatrix} -D_{34}^{(1)} & -D_{35}^{(1)} & D_{31}^{(2)} & D_{32}^{(2)} \\ -D_{64}^{(1)} & -D_{65}^{(1)} & D_{61}^{(2)} & D_{62}^{(2)} \\ -D_{44}^{(1)} & -D_{45}^{(1)} & 0 & 0 \\ 0 & 0 & -D_{41}^{(2)} & -D_{42}^{(2)} \end{pmatrix},$$

$$M = \begin{pmatrix} D_{31}^{(1)} & D_{32}^{(1)} & -D_{34}^{(2)} & -D_{35}^{(2)} \\ D_{61}^{(1)} & D_{62}^{(1)} & -D_{64}^{(2)} & -D_{65}^{(2)} \\ D_{41}^{(1)} & D_{42}^{(1)} & 0 & 0 \\ 0 & 0 & D_{44}^{(2)} & D_{45}^{(2)} \end{pmatrix}.$$

The ordering of the columns of Y corresponds to taking non-zero values of $w_1^{(1)+}$, $w_2^{(1)+}$, $w_1^{(2)-}$ and $w_2^{(2)-}$ in Eqs. (15), in this order, during the derivation of the four systems of equations.

The 16 coefficients appearing in Eq. (16) have been obtained in closed form by solving separately the four systems of equations and using Cramer's method. Algebraic manipulations are greatly simplified by the fact the systems only differ in their right-hand-side vector. Due to the numerous symmetries of the problem, final expressions assume quite simple forms. Making extensive use of the following quantities

$$E_m = 2\mu_m(s_3^{P;m}s_3^{S;m}S + \chi_m^2 S^{-1}),$$

$$F_m = 0.5S^{-1}s_3^{P;m}s_{S;m}^2 \quad m = 1, 2,$$

$$G_m = 2\mu_m(s_3^{P;m}s_3^{S;m}S - \chi_m^2 S^{-1}),$$

$$H = (F_1E_2 + F_2E_1),$$

the coefficients are found to be

$$
\begin{aligned}
&R^{+}_{P\to P} = (E_2F_1 + F_2G_1)H^{-1} \quad R^{+}_{S\to P} = \left(- 4F_2\mu_1 \frac{c_{S;1}}{c_{P;1}} s_3^{S;1}\chi_1 \right) H^{-1},\\
&R^{+}_{P\to S} = \left(4F_2\mu_1 \frac{c_{P;1}}{c_{S;1}} s_3^{P;1}\chi_1 \right) H^{-1} \quad R^{+}_{S\to S} = (-E_2F_1 + F_2G_1)H^{-1},\\
&T^{+}_{P\to P} = \left(4F_1\mu_1 \frac{c_{P;1}}{c_{P;2}} \chi_1\chi_2 S^{-1} \right) H^{-1} \quad T^{+}_{S\to P} = \left(4F_1\mu_1 \frac{c_{S;1}}{c_{P;2}} s_3^{S;1}\chi_2 \right) H^{-1},\\
&T^{+}_{P\to S} = \left(4F_1\mu_1 \frac{c_{P;1}}{c_{S;2}} \chi_1 s_3^{P;2} \right) H^{-1} \quad T^{+}_{S\to S} = \left(4F_1\mu_1 \frac{c_{S;1}}{c_{S;2}} s_3^{S;1} s_3^{P;2} S \right) H^{-1},\\
&R^{-}_{P\to P} = (G_2F_1 + F_2E_1)H^{-1} \quad R^{-}_{S\to P} = \left(4F_1\mu_2 \frac{c_{S;2}}{c_{P;2}} s_3^{S;2}\chi_2 \right) H^{-1},\\
&R^{-}_{P\to S} = \left(- 4F_1\mu_2 \frac{c_{P;2}}{c_{S;2}} s_3^{P;2}\chi_2 \right) H^{-1} \quad R^{-}_{S\to S} = (G_2F_1 - F_2E_1)H^{-1},\\
&T^{-}_{P\to P} = \left(4F_2\mu_2 \frac{c_{P;2}}{c_{P;1}} \chi_1\chi_2 S^{-1} \right) H^{-1} \quad T^{-}_{S\to P} = \left(- 4F_2\mu_2 \frac{c_{S;2}}{c_{P;1}} s_3^{S;2}\chi_1 \right) H^{-1},\\
&T^{-}_{P\to S} = \left(- 4F_2\mu_2 \frac{c_{P;2}}{c_{S;1}} s_3^{P;1}\chi_2 \right) H^{-1} \quad T^{-}_{S\to S} = \left(4F_2\mu_2 \frac{c_{S;2}}{c_{S;1}} s_3^{S;2} s_3^{P;1} S \right) H^{-1},
\end{aligned}
\tag{17}
$$

where $s_3^{P,S;m} = (s^2_{P,S;m} - S^2)^{1/2}$, and $\chi_m = 0.5 s^2_{S;m} - S^2$.

(The coefficients given by Eqs. (17) can be used to study the transmission/reflection of plane waves at a frictionless interface. The incidence of the plane wave is characterized by $S\kappa s_{P,S}$ where κ is the magnitude of the projection in the plane (x_1, x_2) of the unit vector giving the direction of propagation of the plane wave.)

Alternatively, matrix M^{-1} in Eq. (16) can be evaluated by numerical methods. However, if M is ill-conditioned (see Issacson and Keller, 1966), the analytical expressions of the coefficients should be used. It is to note that the numerical evaluation of the coefficients for a welded interface as presented by van der Hijden (1987, p. 30) and for a frictionless interface (see Eq. (16)) yield the same form for the 6×6 matrix of coefficients, i.e., the ordering of the coefficients is the same; it follows that a computer program using the GR theory and an adequate formalism can easily makes use, alternatively, of one condition or the other.

The expressions in Eqs. (17) have been carefully checked with a symbolic manipulation code. A useful check when implementing the coefficients is to compare the results of computations obtained, alternatively, with the analytical expressions Eqs. (17) and by performing the numerical matrix inversion Eq. (16).

All the transmission/reflection coefficients have the same denominator H which appears to be the equation that yields the velocity of interface waves between two media in frictionless contact (see the equation derived by Achenbach and Epstein (1967)). More precisely, the real and positive zero, if any exists, of H is the slowness of the interface wave. For further reference, we introduce

$$\Delta_S = S^2 H = s_3^{P;1} s^2_{S;1} \mu_2 \Delta_{R;2} + s_3^{P;2} s^2_{S;2} \mu_1 \Delta_{R;1}, \tag{18}$$

where

$$\Delta_{R;m} = s_3^{P;m} s_3^{S;m} S^2 + \chi_m^2 \quad m = 1, 2 \tag{19}$$

is the "Rayleigh-wave denominator". The real and positive zero of $\Delta_{R;m}$ is the slowness of the Rayleigh wave at the free surface of half-space 1 or 2 (Achenbach, 1973).

5. Transformation back to the space-time domain

This section presents the basic steps of the tridimensional Cagniard–de Hoop method with application to solutions in the form of Eq. (10) derived in Section 3. Here the method is applied to solutions in a Laplace–Fourier domain which include the transmission coefficients at the *frictionless* interface; as far as the authors know, these form of solutions have never been treated with the Cagniard–de Hoop method, hence a discussion of the analyticity of the integrand, which is crucial in the method, is provided.

The derivation of the transform domain solution presented in Sections 3 and 4 is independent of the location of the receivers and of the mechanical parameters of the media. In contrast, the transformation back to the space-time domain is not. As a matter of fact, the application of the CdH method is more or less complex depending on the location of the receiver with respect to the source of waves. The presentation of the method in this section is restricted to the calculation of body waves contributions to the wave field; in particular, the treatment of head waves is not described (see van der Hijden (1987) for other technical aspects of the method). The discussions provided focuses on the features of the method specifically concerned with the interface contact conditions.

The contribution in the space-time domain of one GR is the inverse Laplace transform of Eq. (10). The first step of the three-dimensional CdH method (de Hoop, 1960) is to perform the following substitution

$$\mathrm{i}k_1 = s\cos\theta - \mathrm{i}q\sin\theta, \quad \mathrm{i}k_2 = s\sin\theta + \mathrm{i}q\cos\theta,$$

where q is a real number and s can be a complex number. Variables θ and r ($0 \leqslant \theta \leqslant 2\pi$ and $0 \leqslant r < \infty$) are the polar coordinates in the (x_1, x_2) plane

$$x_1 = r\cos\theta, \quad x_2 = r\sin\theta.$$

All the quantities appearing in the integrand must be rewritten in terms of s and q; in particular we now have

$$s_3^{P,S} = (s_{P,S}^2 - s^2 + q^2)^{1/2}. \tag{20}$$

Noting that $\mathrm{i}k_1x_1 + \mathrm{i}k_2x_2 = sr$, Eq. (10) is rewritten

$$\hat{b}_j^{\alpha\to\beta}(\mathbf{x}, p) = \hat{\phi}(p) \times \mathrm{i}\Big(\frac{p}{2\pi}\Big)^2 \int_{-\infty}^{\infty} \mathrm{d}q \int_{-\mathrm{i}\infty}^{\mathrm{i}\infty} B_j^{\alpha\to\beta}(s,q) T_{\alpha\to\beta} \exp[-p(sr + s_3^{\alpha;1}h_1 + s_3^{\beta;2}h_2)]\,\mathrm{d}s. \tag{21}$$

In Eq. (21), the integration over the variable s lies along the imaginary axis; the CdH method consists in performing the integration over s along a contour in the complex s-plane away from the imaginary axis. This requires to extend the definition of the integrand in the complex s-plane by analytic continuation. In order to keep the square roots (see Eq. (20)) single valued, we take $\mathrm{Re}[s_3^{P,S;1,2}] \geqslant 0$, where Re denotes the real part of a quantity. Due to the terms $s_3^{P,S;1,2}$ in the integrand, height branch points occur on the real axis at $S^{P,S;1,2} = (s_{P,S;1,2}^2 + q^2)^{1/2}$ and at $-S^{P,S;1,2}$. In accordance with the conditions put on the square-root expressions, the s-plane is supplemented with branch cuts along $S^{P,S;1,2} < |\mathrm{Re}[s]| < \infty$ and $\mathrm{Im}[s] = 0$, where Im denotes the imaginary part of a quantity. The cut s-plane is shown in Fig. 3.

A new contour of integration, the—so-called—CdH contour, is defined (for each GR) by

$$\tau = sr + s_3^{\alpha;1}h_1 + s_3^{\beta;2}h_2, \tag{22}$$

where τ is a real positive parameter with the dimension of time. The contour $s(\tau)$ is, in the general case, complex and runs from $\tau = T(q)$ (the minimum of τ on the contour, defined below) to $\tau = \infty$. The "origin" of the contour is on the real axis and is denoted by $s_0(q) = s(\tau = T(q))$. A typical contour $(-\mathscr{C})$ in the s-plane is depicted in Fig. 3 (here we have used $-\mathscr{C}$, instead of $\mathscr{C}$, to indicate that the CdH contour, as indicated on the figure, is followed in the direction of decreasing τ).

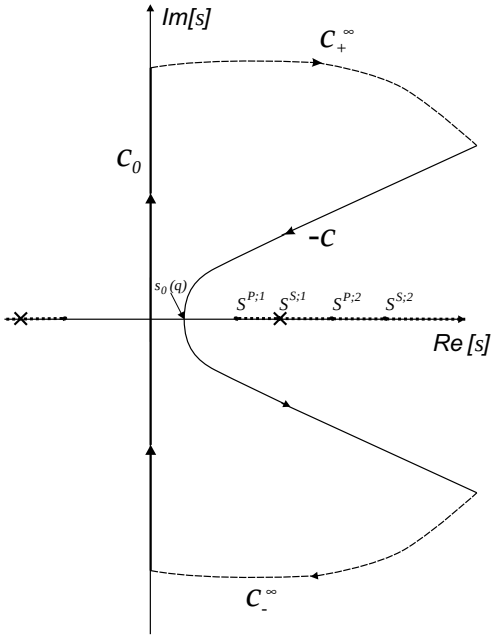

Fig. 3. Contour Γ in the s-plane used for the application of Cauchy's theorem. $\mathscr{C}_0$ is the original contour and $\mathscr{C}$ is the Cagniard–de Hoop contour. Branch cuts are represented in thick discontinuous lines; the four branch points with positive real part and the pole at $(s_{S;1}^2 - q^2)^{1/2}$ are shown.

The application of Cauchy's theorem involves a closed contour of integration shown in Fig. 3: $\Gamma = \mathscr{C}_0 + \mathscr{C}_+^\infty + \mathscr{C}_-^\infty - \mathscr{C}$, where $\mathscr{C}_0$ is the original contour along the imaginary axis and $\mathscr{C}_\pm^\infty$ are circular arcs of arbitrarily large radius, centered at the origin of the complex plane. If no singularity is enclosed in Γ, Cauchy's theorem states that the integration over Γ is zero; invoking Jordan's Lemma, it can be shown that integrals along $\mathscr{C}_+^\infty$ and $\mathscr{C}_-^\infty$ are zero, so that the integrals over $\mathscr{C}_0$ and $\mathscr{C}$ are equivalent. Two types of singularity may be enclosed in Γ: branch cuts and poles. With regards to the branch cuts, if the "origin" of the contour $s_0(q)$ is located at the left of the leftmost branch point, nothing happens, otherwise Γ must be deformed so that the branch cut remains outside Γ. Furthermore, Γ must be chosen so that all the poles of the integrand lie outside it. It is to note that the CdH contour itself, as defined by Eq. (22), is not perturbed by the presence of singularities inside the original contour Γ; if deformations of Γ are necessary, new terms (integral along branch cuts and/or residues) must be calculated and added to the integral calculated along the CdH contour.

In the expression of a GR as given by Eq. (10), the term $T_{\alpha\to\beta}$ may induce a pole if its denominator vanishes. It is well-known that real roots of the denominators of transmission/reflection coefficients are associated with interface waves. Typical examples are Stoneley waves at a welded interface between to elastic media (see Cagniard, 1962, p. 42; Eringen and Suhubi, 1975, p. 539), Scholte waves at the interface between a solid and a fluid (see de Hoop and van der Hijden, 1983) and Rayleigh waves at the free surface of a half-space (Achenbach, 1973, p. 189). Depending on the nature of the interface, they are more or less restrictive conditions on the material properties for interface waves to exist. Unlike for Scholte and Rayleigh waves, the conditions for propagation of Stoneley waves are rather restrictive, i.e., good mechanical coupling is required between the media at the interface (see Cagniard, 1962).

The conditions, with respect to the material properties, for existence of interface waves at the frictionless sliding contact have been discussed by Achenbach and Epstein (1967); in other words, they gave a condition

for the occurrence of poles of the transmission/reflection coefficients on the *real* axis (that is, for the zeros of Δ_S, as given by Eq. (18)). But the occurrence of zeros of Δ_S *everywhere* in the complex S-plane must still be elucidated.

It is seen from Eq. (18) that if media 1 and 2 are identical, the equation $\Delta_S = 0$ reduces to the well-known Rayleigh wave equation $\Delta_R = 0$ which has known analytical solutions (two opposite real roots). For the material configuration of interest in the present paper where the two media are different, the occurrence of zeros of Δ_S in the complex S-plane is elucidated in the Appendix A. With the help of the Principle of the Argument (PA) from complex function theory, it is shown that Δ_S has no zero in the entire complex S-plane. In particular, there is no zero on the real axis, hence no interface wave (this result is consistent with the condition for the existence of interface waves given by Achenbach and Epstein (1967)).

For the configuration of the present study, we may have for rays *SP* and *SS* $S^{P;1} < s_0(q) < S^{S;1}$, such that the CdH contour intersects a branch cut. From a physical point of view, this implies that a part of the incident energy has travelled from the source to the receiver in a shorter time than body waves (the wave fronts corresponding to the body waves, and the associated arrival times, are consistent with the geometrical ray theory). This energy is carried by the so-called head waves. The amplitude of head waves is calculated as follows: in an expression in the form of Eq. (21) the integration for s along the imaginary axis is replaced by an integration along the real part of the CdH contour $s(\tau)$ that runs along the branch cut, from $S^{P;1}$ to $s_0(q)$. For more detail on the calculation of head wave contributions, see van der Hijden (1987); the mathematical expressions that follow are concerned with body waves only.

Two opposite poles (for the GRs $\hat{b}_j^{S\to P}$ and $\hat{b}_j^{S\to S}$ only) at $s = \pm S^{S;1}$, induced by the amplitude factor $W_5^{(1)}$ given by Eq. (9), are located on the branch cuts and are never inside Γ. This closes the discussion of the singularities that may occur inside Γ and Cauchy's theorem can be applied on the contour $\Gamma = \mathscr{C}_0 + \mathscr{C}_+^\infty + \mathscr{C}_-^\infty - \mathscr{C}$ depicted in Fig. 3.

The contour $-\mathscr{C}$ being symmetric with respect to the real axis, we split it into two symmetric parts $-\mathscr{C}_\tau$ and $\mathscr{C}_\tau^*$ ($-\mathscr{C} = -\mathscr{C}_\tau + \mathscr{C}_\tau^*$), where $-\mathscr{C}_\tau$ is the path with positive imaginary part and $\mathscr{C}_\tau^*$ is its counterpart with negative imaginary part. Denoting

$$A(s,q) = B_j^{\alpha\to\beta}(s,q)T_{\alpha\to\beta}(s,q),$$

Cauchy's theorem for the integral over s in Eq. (21) gives

$$\begin{aligned}
&-\int_{-\mathrm{i}\infty}^{\mathrm{i}\infty} A(s,q)\exp[-p(sr + s_3^{\alpha;1}h_1 + s_3^{\beta;2}h_2)]\,\mathrm{d}s \\
&\quad = \int_{-\mathscr{C}_\tau} A(s,q)\exp[-p\tau(s)]\,\mathrm{d}s + \int_{\mathscr{C}_\tau^*} A(s,q)\exp[-p\tau(s)]\,\mathrm{d}s \\
&\quad = -\int_{\mathscr{C}_\tau} A(s,q)\exp[-p\tau(s)]\,\mathrm{d}s + \int_{\mathscr{C}_\tau} A(s^*,q)\exp[-p\tau(s^*)]\,\mathrm{d}s,
\end{aligned}$$

where s^* is the complex conjugate of s. Due to symmetry relations (Schwarz's reflection principle) $A(s^*,q) = A^*(s,q)$, and $\tau(s^*) = \tau(s)$; using $A - A^* = 2\mathrm{i}\,\mathrm{Im}[A]$, the integration on the imaginary axis in Eq. (21) is replaced by an integration over τ such that

$$\hat{b}_i^{\alpha\to\beta}(\mathbf{x},p) = \hat{\phi}(p) \times \frac{p^2}{2\pi^2}\int_{-\infty}^{\infty}\mathrm{d}q\int_{T(q)}^{\infty}\mathrm{Im}[B_i^{\alpha\to\beta}(s,q)T_{\alpha\to\beta}(s,q)\partial_\tau s]\exp[-p\tau]\,\mathrm{d}\tau, \tag{23}$$

where $T(q)$ is given by (van der Hijden, 1987)

$$T(q) = \frac{(s_{\alpha;1}^2 + q^2)^{1/2}h_1}{\cos\Theta_1(q)} + \frac{(s_{\beta;2}^2 + q^2)^{1/2}h_2}{\cos\Theta_2(q)}, \tag{24}$$

and may be thought of as the travel time, from the source to the receiver, of a wave travelling with slownesses $(s^2_{\alpha;1}+q^2)^{1/2}$ and $(s^2_{\beta;2}+q^2)^{1/2}$ in media 1 and 2, respectively. The terms $\Theta_i(q)$, which may be compared to the angles of geometrical rays with respect to the interface obtained following Snell's law, are defined through the two equations

$$(s^2_{\alpha;1}+q^2)^{1/2}\sin\Theta_1(q)=(s^2_{\beta;2}+q^2)^{1/2}\sin\Theta_2(q)=s^0(q),$$
$$r=h_1\tan\Theta_1(q)+h_2\tan\Theta_2(q).$$

The final step of the three-dimensional CdH method is to interchange the integrations over s and q in Eq. (23). The new limits are $-Q(\tau)$ and $Q(\tau)$ which are solutions for q of $\tau=T(q)$. A GR contribution in the Laplace-domain is

$$\hat{b}_i^{\alpha\to\beta}(\mathbf{x},p)=\hat{\phi}(p)\frac{p^2}{2\pi^2}\int_{T_a}^{\infty}\left\{\int_{-Q(\tau)}^{Q(\tau)}\mathrm{Im}[B_i^{\alpha\to\beta}(s,q)T_{\alpha\to\beta}(s,q)\partial_\tau s]\,\mathrm{d}q\right\}\exp[-p\tau]\,\mathrm{d}\tau, \tag{25}$$

where $T_a=T(q=0)$ is the arrival time of the geometrical wave front associated with the GR. In Eq. (25), the integration over τ has the form of a forward Laplace transform and the space-time domain solution is obtained by inspection:

$$\begin{cases} b_j^{\alpha\to\beta}(\mathbf{x},t)=0 \quad \text{for } 0\leqslant t\leqslant T_a,\\ b_j^{\alpha\to\beta}(\mathbf{x},t)=\frac{1}{2\pi^2}\partial_{tt}\phi(t)*\int_{-Q(t)}^{Q(t)}\mathrm{Im}[B_j^{\alpha\to\beta}(s,q)T_{\alpha\to\beta}(s,q)\partial_t s]\,\mathrm{d}q \quad \text{for } T_a<t, \end{cases} \tag{26}$$

where (in this equation only) $*$ denotes the temporal convolution. Note that for $\phi(t)=H(t)$, where $H(t)$ is the Heaviside step function, no convolution is required to calculate the displacements in the medium.

The method has been implemented in a computer program. The computational scheme used to derive the numerical results shown in the next section was presented in a former paper (Grimal et al., 2002a).

6. Results

The original numerical results presented in this section are both (i) an illustration of the potential of the method for the characterization of a transient wave field transmitted at an interface (ii) a quantification of the differences of the transmitted wave fields for welded and frictionless contact conditions in the case of a *weakly coupled* bimaterial that represents the thorax (Section 1).

All the responses have been computed at receivers in medium 2, for a point force in along $\mathbf{x}_3$ buried in medium 1 at two centimeters below the interface ($x_I=0.02$ m).

Three bimaterials, each associated with a set of mechanical properties given in Table 1, have been considered:

Table 1
Lamé's coefficients, densities and wave speeds for media 1 and 2

	$\lambda\times10^6$ (Pa)	$\mu\times10^6$ (Pa)	ρ (kg m^{-3})	c_S (m s^{-1})	c_P (m s^{-1})
Medium 1 (Case I–III)	1126	562	1000	750	1500
Medium 2 (Case I)	1126	562	1000	750	1500
Medium 2 (Case II)	34	8	800	100	250
Medium 2 (Case III)	0.034	0.008	500	4	10

c_S and c_P are the pressure and shear waves speeds.

- Case I, where the two media have the same mechanical properties, is used as a reference—in this case the acoustic coupling is optimum;
- in Cases II and III, medium 2 is "compliant" in comparison with medium 1, that is, the wave speeds in medium 1 are much larger than those in medium 2—in Case III, medium 2 is very compliant, so that the two media are said to be weakly coupled. The values of the mechanical parameters in Case III correspond to the thoracic wall and the lung.

Each of the Figs. 4 (Case II) and 5 (Case III) displays the displacements, due to a step of force ($\phi(t) = H(t)$, where $H(t)$ denotes the Heaviside step function), at two receivers A and B, for both a *welded* interface (thin line) and a *frictionless* interface (bold line). Results are given in the plane $(O; \mathbf{x}_1, \mathbf{x}_3)$. Receiver A is placed at $x_1 = 0.025$ m, $x_3 = 0.025$ m and receiver B is placed at $x_1 = 0.025$ m, $x_3 = 0.07$ m; the curves corresponding to receiver B are associated with the largest arrival time and with smaller amplitudes.

At the source level, in medium 1, both a *P*- and a *S*-wave are generated. These waves are transmitted in medium 2, with or without wave conversion so that four wave arrival times (*PP*, *SP*, *PS* and *SS*) are manifest at the receivers. We have mentioned on the plots, the arrival times of each GR contribution—each wave—by an arrow and two letters. The responses include a head wave contribution for rays *SP* and *SS* at both receivers A and B in cases II and III. Head waves contributions act during a finite time window; head waves arrive shortly before the body wave and end shortly after the arrival of the body wave. In every case, head waves amplitudes are very small in comparison to body waves amplitudes. The arrival times of rays *PP* and *SP* on the one hand, and of rays *PS* and *SS* on the other hand are hardly distinguishable. This is due to the relatively low wave speeds in medium 2. (Note that the arrival times for both frictionless and welded contacts are the same: they are basically given by Eq. (24), with $q = 0$, and do not depend on the transmission coefficients.) The static responses have also been evaluated by computing responses for large times, these are drawn as straight lines on the right of the plots.

Some characteristics of the wave patterns are describe in what follows. The differences between the two interface configurations are more obvious in plots of u_1; indeed, *S*-waves—which are the more influenced by the nature of the interface—contribute for a large part to u_1. The displacement u_3 is slightly larger for the frictionless interface. The differences in the static value attained, for the two contact conditions, is different

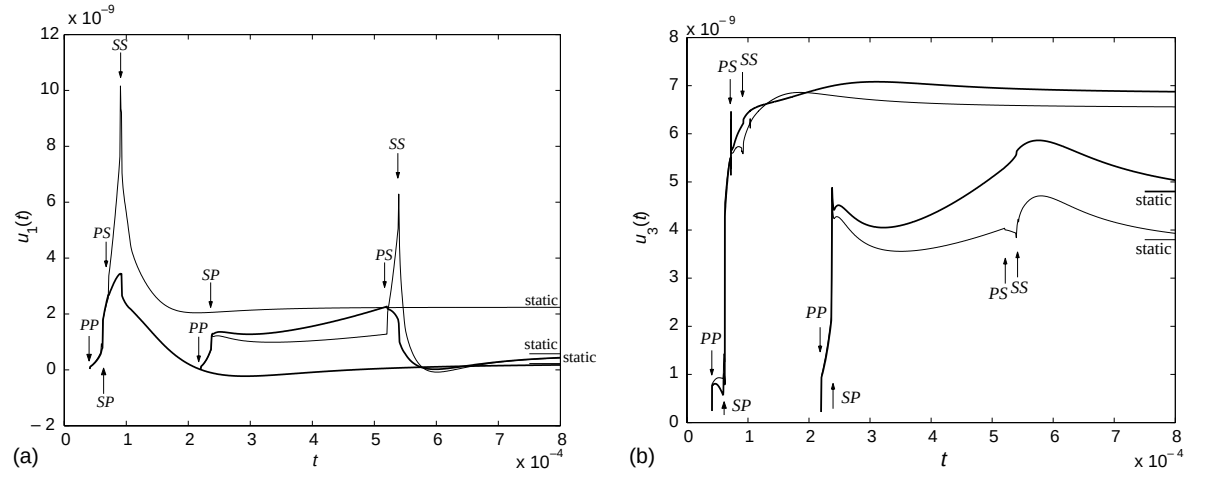

Fig. 4. Case II, transient displacements in a bimaterial subjected to a buried point force, at receivers A and B, for a welded (thin line) and a frictionless interface (bold line). The signal reaches receiver A (two curves on the left) before receiver B (two curves on the right). (a): $u_1(t)$; (b): $u_3(t)$.

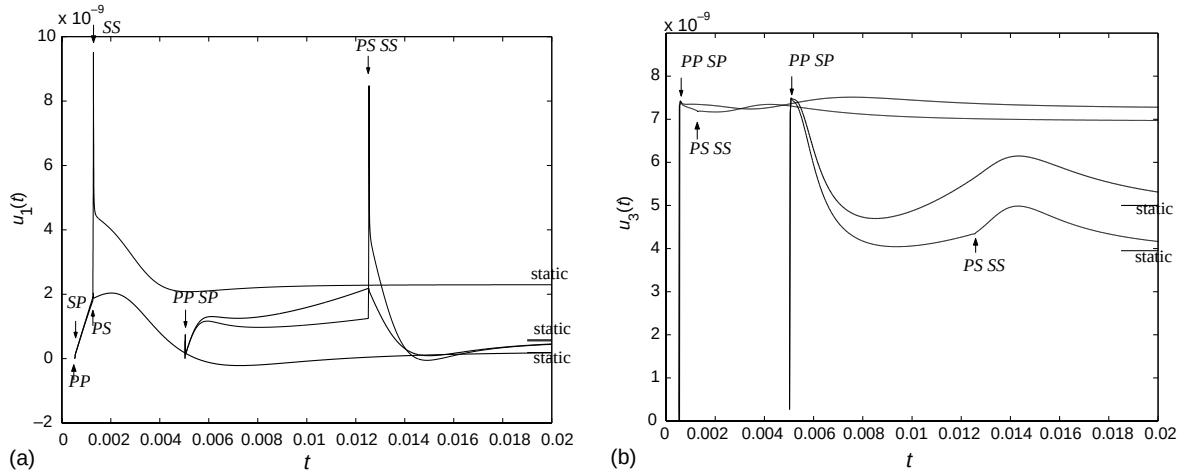

Fig. 5. Case III, same caption as Fig. 4. (a): $u_1(t)$; (b): $u_3(t)$.

for u_1 and u_3, and depends on the distance of the receiver from the interface. The response times (times before static values are attained) between the welded interface configuration and the frictionless interface configuration are not very different; in contrast, calculations for Case I (plots not reproduced here) indicated that for identical media on each side of the interface, response times are increased for the frictionless contact. From a physical point of view, these differences in response times and amplitudes of the static displacements are probably due to the additional degree of freedom added in the bimaterial by allowing sliding. It is manifest on Figs. 4 and 5a that *PS*-waves, and to a lesser extent *SS*-waves, are the more influenced by the contact conditions; the contribution of these waves to the response is less for the frictionless interface and this effect is all the more pronounced that the acoustic coupling is weak. This trend was also observed in the case where only *P*-waves are incident at the interface (waves are generated by a source of strain rate, plots not reproduced here).

Repartition of energy. A product of the components of vector **b** yields $P_3 = v_1\sigma_{13} + v_2\sigma_{23} + v_3\sigma_{33}$, which is the component in direction x_3 of the Poynting vector (energy flux). In Grimal et al. (2002a), it was pointed out that P_3 is an approximation of the density of strain energy, valid in the material configuration used in the present study. Fig. 6 shows plots of $P_3(t)$ obtained for an impulse of duration 300 μs modeled by a four point optimum Blackman window (see van der Hijden, 1987 or Grimal et al., 2002a) for Case II (Fig. 6a) and Case III (Fig. 6b). Plots are presented for receivers B (for Case II) and A (for Case III), chosen for clarity reasons; the discussion that follows is equivalent for both receivers location. It is manifest in Fig. 6 that the energy arrives in two distincts bundles, the first is associated with *P*-waves and the second with *S*-waves; even very close to the interface, the two bundles are well-separated because of the low wave speeds in medium 2 (however, arrival times of waves *PP* and *SP* on the one hand, and of waves *PS* and *SS* on the other hand, are indistinguishable). The main features extracted from these plots are (1) *S*-waves contributions in medium 2 are less in the case of a frictionless interface, and in Case III, these contributions approach zero; (2) in contrast, the *P*-waves contributions are weakly influenced by the interface condition, and in Case III, the *P*-wave part of the responses for frictionless and welded contact are undistinguishable. Observations (1) and (2) are consistent with the results described above for the displacements histories.

The plots of Fig. 7 have been obtained in Case III as follows: for several receiver locations $P_3(t)$ was calculated, plots like those reproduced in Fig. 6 were drawn and the maxima of, on the one hand the *P*-waves part, and on the other hand the *S*-waves part, were collected. This was done for the two contact

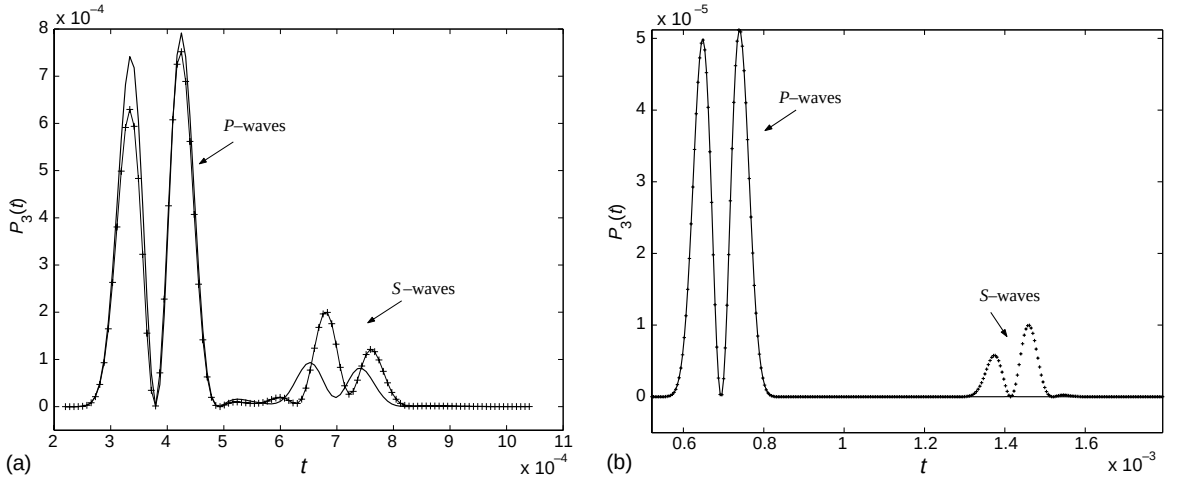

Fig. 6. Examples of plots of $P_3(t)$. (a) Case II for receiver B ($x_1 = 0.025$, $x_3 = 0.07$), welded contact (thin line with +), frictionless contact (thick line); (b) Case III, receiver A ($x_1 = x_3 = 0.025$), welded contact (+), frictionless contact (thick line).

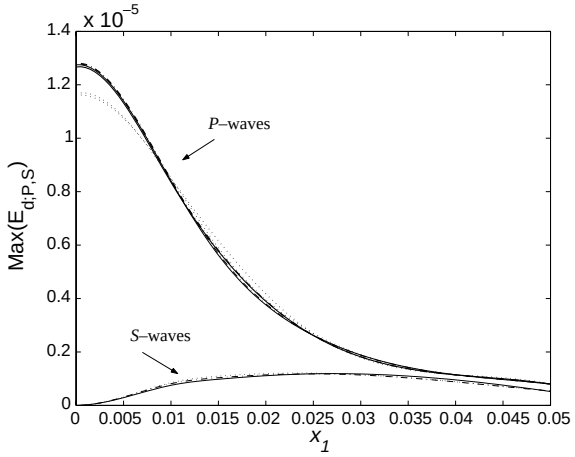

Fig. 7. Case III, repartition of the maxima of strain energies associated with *P*- and *S*-waves during the passage of a pulse in medium 2. Thick and thin lines (or dots) are associated with frictionless and welded contact, respectively. Each line corresponds to a fixed x_3. — $x_3 = 0.0.25$; $-\cdot-$ $x_3 = 0.04$; $\cdots$ $x_3 = 0.01$.

conditions. Then the values of P_3 were converted to a density of strain energy E_d upon using the formula $E_d^{P,S} = 0.5 s_{P,S} P_3^{P,S}$. Fig. 7 is a "map" of the values of E_d in medium 2 (see also Fig. 7b of Grimal et al. (2002a)); on the figure, each line represents the normalized maxima at a given value of x_3, for $0 < x_1 < 5$ cm. Thick and thin lines are associated with frictionless and welded conditions, respectively. The observations (1) and (2) described for plots of $P_3(t)$ in Fig. 6 are confirmed for a certain range of receiver locations.

Transmission of plane waves. Fig. 8 shows the variation of the transmission coefficients with the incidence of plane waves at frictionless and welded interfaces, for the three material configurations of Cases I, II and III. For the sliding contact, coefficients given in Eqs. (17) have been used with $0 < \mathrm{Re}[S] < s_{P;1}$ and $\mathrm{Im}[S] = 0$. The relative values of the coefficients indicated on the figure are consistent with the previous

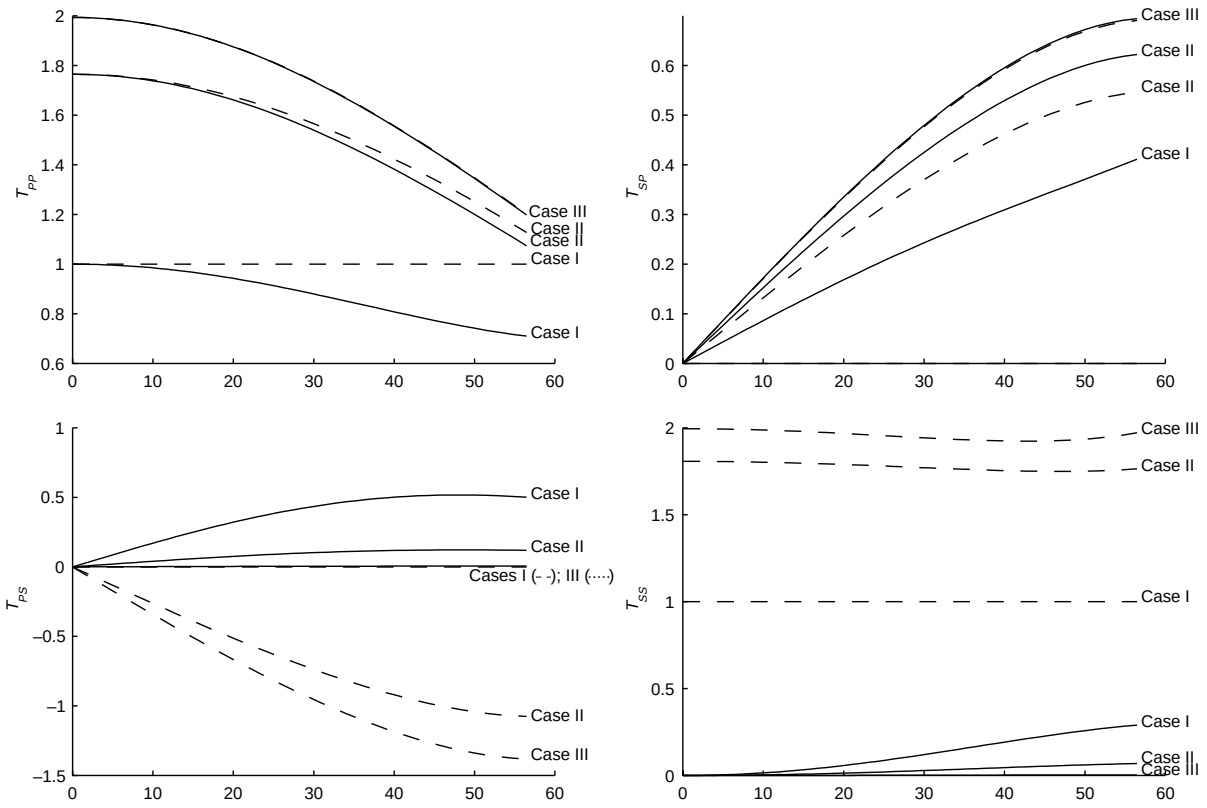

Fig. 8. Variation of transmission coefficients with incidence of plane waves at frictionless/welded interfaces. The incidence of plane waves is indicated in degree on the abscissa. Cases I, II and III, in this order, correspond to media with decreasing acoustic coupling. – welded contact; — frictionless contact.

remarks: Observation (1) is consistent with the fact that with the weak-coupling the values of the coefficients $T_{P\to S}$ and $T_{S\to S}$ for the frictionless contact get small. Observation (2) is consistent with the fact that with the weak-coupling the curves of the coefficients $T_{P\to P}$ and $T_{S\to P}$ for welded and frictionless contact get close.

7. Discussion and conclusions

The results presented above elucidate the phenomena of transmission of spatially curved elastic waves at a frictionless sliding interface between two weakly coupled elastic media. While qualitative results can be obtained straightforward in many problems upon using transmission coefficients of plane waves, the derivation of quantitative results in some practical cases when the waves are generated at a finite distance from the interface is a complicated problem. The Generalized rays/Cagniard–de Hoop method is a good candidate to calculate responses in these cases: solutions including near and far field contributions, and possibly non-geometric waves and interface waves, are derived, allowing for a detailed investigations of the wave field. For the specific application considered in this work, only some features of the powerful method have been used; the main benefit was to work with Green's function which are valid whatever the frequency content of the pulse and the distances to the interface.

The transmission/reflection coefficients at the frictionless sliding interface, required by the method, have been derived in closed form; an alternative procedure to compute the coefficients with a numerical method is also given. The application of Cauchy's theorem in the CdH method has required a detailed mathematical analysis of the newly derived transmission coefficients, the conclusion of this analysis is that no complex pole occurs for Cases II and III.

Note that an elaborated contact condition—linear slip interface—has been recently considered by Verweij and Chapman (1997) in association with the CdH method. However, the contact condition intended at modeling a fracture and the media in contact had the same mechanical properties; in this case, part of the analysis is greatly simplified, just as in Case I.

Complex models of the thorax (which are supposed to be more realistic than the idealized model considered here) are currently developed relying on the finite elements method; one of the questions that arise in the numerical modeling is the nature of the contact conditions that must be assumed between the various tissues in the thorax and in particular between the thoracic wall and the lung. With regard to a straightforward engineering application, the motivation of the work presented in this paper is to quantify the influence of the nature of the contact condition assumed at the interface between the thoracic wall and the lung.

According to a discussion presented in Grimal et al. (2002a), the energy flux in the $\mathbf{x}_3$ direction is a possible criterion for evaluating the risk of lung injury. Results shown in Figs. 4–7 indicate that (i) the energy flux in the lung associated with S-waves disappears with the frictionless contact conditions and that (ii) the energy flux in the lung associated with the P-waves weakly depends on the contact condition. Furthermore, the results indicate that the "elimination" of the S-waves contributions basically is effective because the acoustic coupling between the media in contact (the thoracic wall and the lung) is weak.

The main conclusion relative to the biomechanical problem follows: if frictionless sliding contact is the suitable physiological condition at the thoracic wall-lung interface, there is little chance that S-waves are responsible of lung injury since they only carry a very small part of the energy transmitted.

Acknowledgements

The authors would like to thank the "Délégation Générale pour l'Armement" of the Minister of Defense of France for supporting this work.

Appendix A. Poles of the transmission coefficients (determination of the roots of Δ_S)

In this Appendix A we show, by using the Principle of the Argument (PA) from complex function theory, that the transmission/reflection coefficients at the frictionless interface given by Eqs. (17) have no pole in the entire complex S-plane for the material properties corresponding to Cases II and III of Section 6.

Obviously, the poles of the transmission coefficients are the zeros of Δ_S. These roots, in the general case, can only be obtained with the help numerical methods, so the PA is very helpful in giving the number of solutions.

It is convenient to calculate the number of zeros of $\overline{\Delta}_S = \Delta_S / s_3^{P;1}$ instead of the number of zeros of Δ_S, so that the branch cuts of the analyzed quantity remain bounded. We restrict the analysis to the case where $s_{P;1} < s_{S;1} < s_{P;2} < s_{S;2}$, as it is the case for Cases II and III of Section 6.

By taking $\mathrm{Re}[s_3^{P,S;1,2}] \geqslant 0$, the function $\overline{\Delta}_S$ is single valued in the cut S-plane shown in Fig. 9. Eight branch points occur at $\pm s_{P,S;1,2}$, the associated branch cuts are taken along the real axis between branch points $s_{P;1}$ and $s_{S;2}$, and between $-s_{P;1}$ and $-s_{S;2}$. The function $\overline{\Delta}_S(S)$ is holomorphic in the entire cut S-plane; note that $\overline{\Delta}_S(S)$ has only one pole at the branch point $S = s_{P;1}$, hence outside the cut S-plane.

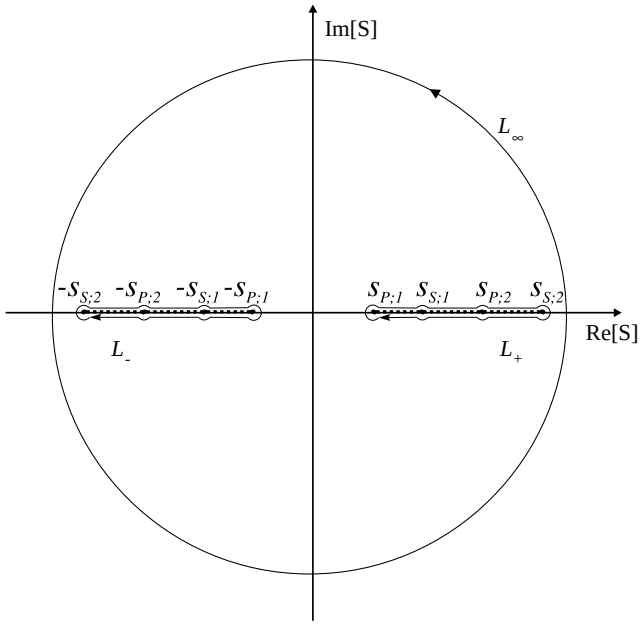

Fig. 9. Contours in the S-plane used for the application of the Principle of the Argument to determine the number of poles of the reflection/transmission coefficient. The two branch cuts are represented in thick discontinuous lines.

The PA is a direct consequence of Cauchy's residue theorem of the theory of complex variables (see Dieudonné, 1980, p. 244; LePage, 1961, p. 211) which may be stated as follows. Let L be a simple closed curve followed in the positive (anticlockwise) direction (i.e., L is a Jordan curve) in a simply connected domain; let $f(z)$ be holomorphic everywhere inside L except at a finite number of poles; and $f(z)$ has no poles or zeros on L. If Z and N respectively denote the number of zeros and poles, counted with multiplicities, inside L, then

$$Z - P = \frac{1}{2\pi \mathrm{i}} \int_L \frac{f'(\xi)}{f(\xi)}\, \mathrm{d}\xi.$$

Choosing L in the cut S-plane, the PA, with $f = \overline{\Delta}_S$, gives the number of zeros (the domain inside L is free of pole). Using the convention that the square root sign ($\sqrt{}$) designates the radical with positive real part, $\overline{\Delta}_S$ is given by

$$\begin{aligned}\overline{\Delta}_S(S) = {} & s_{S;1}^2 \mu_2 \left[(0.5 s_{S;2}^2 - S^2)^2 - S^2 \sqrt{s_{P;2}^2 - S^2} \sqrt{s_{S;2}^2 - S^2} \right] \\ & + s_{S;2}^2 \mu_1 \frac{\sqrt{s_{P;2}^2 - S^2}}{\sqrt{s_{P;1}^2 - S^2}} \left[(0.5 s_{S;1}^2 - S^2)^2 - S^2 \sqrt{s_{P;1}^2 - S^2} \sqrt{s_{S;1}^2 - S^2} \right]. \end{aligned} \tag{A.1}$$

Through the relation

$$v = \overline{\Delta}_S(S),$$

the S-plane is mapped onto the v-plane. The image of L in the v-plane is denoted by L_v. The PA in the v-plane is written

$$Z = \frac{1}{2\pi \mathrm{i}} \int_{L_v} \frac{\mathrm{d}v}{v}. \tag{A.2}$$

The integrand $1/v$ has only one pole at $v = 0$, hence Z is the number of times L_v encircles the origin of the v-plane. The Jordan curve L, in the S-plane, used for the application of the PA is shown in Fig. 9 L is built as follows: L_∞ is a circle, followed in the positive direction, with center at the origin and arbitrarily large radius; L_+ and L_- are two paths, followed in the negative direction, arbitrarily close to the branch cuts on the positive and negative real axis respectively, which include circular loops of arbitrarily small radius around each branch points (L_+ and L_- are represented in Fig. 9 at a certain distance from the real axis but, in the calculations, quantities are evaluated *on* the real axis). It is important to check that the real and imaginary parts of Δ_S do not cancel together on the cuts, which is the case here. So that the PA can be applied, L must be a closed curve. Hence two arbitrarily chosen paths should be drawn to link L_+ and L_- to L_∞; as long no zeros lie on these paths, nor inside the domain they delimit—and such paths can always be drawn—, the integration Eq. (A.2) along them is zero. Finally, the contour for the application of the PA reduces to $L = L_\infty + L_+ + L_-$.

Contour L_∞: For $|S|$ large (using $(\epsilon - 1)^{1/2} = \mathrm{i}(1 - \epsilon/2) + \mathrm{O}(\epsilon^2)$ and $(1 - \epsilon/2)^2 = 1 - \epsilon + \mathrm{O}(\epsilon^2)$, where ϵ is a small parameter), Eq. (A.1) becomes

$$\overline{\Delta}_S(S) = -0.5S^2 \left[s_{S;1}^2 \mu_2 (s_{P;2}^2 - s_{S;2}^2) + s_{S;2}^2 \mu_1 (s_{P;1}^2 - s_{S;1}^2) \right]. \tag{A.3}$$

Eq. (A.3) indicates that the image of L_∞ in the v-plane encircles the origin twice in the positive direction; hence, denoting by $L_{v,\infty}$ the image of L_∞

$$\frac{1}{2\pi \mathrm{i}} \int_{L_{v,\infty}} \frac{\mathrm{d}v}{v} = 2. \tag{A.4}$$

Contours $L_\pm$: Since $\overline{\Delta}_S$ is only a function of S^2, calculations for L_+ and L_- are identical. Furthermore, $\overline{\Delta}_S$ satisfies Schwarz's reflection principle (i.e., $\overline{\Delta}_S(S^*) = \overline{\Delta}_S(S)^*$, where S^* is the complex conjugate of S), so that the images of the parts of the paths below and above the cut are symmetric with respect to the real axis.

For the calculation of the images of the paths around the branch cuts, we restrict the analysis to the part of L_+ above the cut. Regarding the circular arcs, only the image of the circle around the branch point—and pole—$s_{P;1}$ contributes to the integral. Taking $S = s_{P;1} + \epsilon \mathrm{e}^{\mathrm{i}\theta}$ and letting ϵ go to zero, it is found that the image in the v-plane is a semi-circle followed in the positive position.

Following the path on the real axis for $s_{P;1} < S < s_{S;2}$, and using the notation "PR" for "positive real" and "NI" for "negative imaginary", the radicals are as follows

$$s_{P;1} < S < s_{S;1} \begin{cases} s_3^{P;1}, \mathrm{NI} \\ s_3^{S;1}, \mathrm{PR} \\ s_3^{P;2}, \mathrm{PR} \\ s_3^{S;2}, \mathrm{PR} \end{cases}; \quad s_{S;1} < S < s_{P;2} \begin{cases} s_3^{P;1}, \mathrm{NI} \\ s_3^{S;1}, \mathrm{NI} \\ s_3^{P;2}, \mathrm{PR} \\ s_3^{S;2}, \mathrm{PR} \end{cases}; \quad s_{P;2} < S < s_{S;2} \begin{cases} s_3^{P;1}, \mathrm{NI} \\ s_3^{S;1}, \mathrm{NI} \\ s_3^{P;2}, \mathrm{NI} \\ s_3^{S;2}, \mathrm{PR} \end{cases}. \tag{A.5}$$

Collecting the results of Eq. (A.5) in Eq. (A.1), the image of the path L_+ can be drawn. Fig. 10 shows schematically the image of the loop around a branch cut, as obtained for the examples presented in Section 6.

For Cases II and III of Section 6, the images of the loops L_+ and L_- (followed in the *negative* direction) each encircle the origin of the v-plane once in the *positive* direction, i.e., denoting by $L_{v,\pm}$ the images of $L_\pm$

$$\frac{1}{2\pi \mathrm{i}} \int_{L_{v,\pm}} \frac{\mathrm{d}v}{v} = -1. \tag{A.6}$$

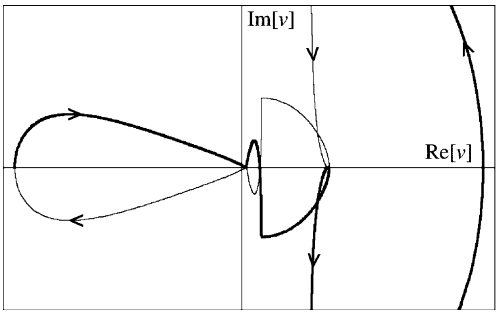

Fig. 10. The typical shape of the image in the v-plane of one of the loops L_+ or L_- (see Fig. 9) around a branch cut in the S-plane. The contour—which closes outside the frame—encircles the origin once in the negative direction. The thin and thick lines correspond to the paths above and below the cut, respectively; the semi-circle on the left is the image of the circle around the pole $s_{P;1}$ of $\overline{\Delta}_S$.

Contour $L = L_\infty + L_+ + L_-$: Collecting the results of Eqs. (A.4) and (A.6), the number of zeros of $\overline{\Delta}_S$ is $Z = 2 - 1 - 1 = 0$, for Cases II and III of Section 6. The calculations of image contours, as presented in this Appendix A, should be performed for each set of material properties considered. An analysis of the general case, of limited practical interest because resulting in many cases depending on the relative magnitude of all the parameters, may also be considered. In conclusion, the calculations presented in this Appendix A prove that for Cases II and III of Section 6, Δ_S has no zero in the entire complex S-plane.

References

Achenbach, J.D., Epstein, H.D., 1967. Dynamic interaction of a layer and a half-space. Journal of the Engineering Mechanics Division EM5, 27–42.

Achenbach, J.D., 1973. Wave Propagation in Elastic Solids. North-Holland, Amsterdam.

Aki, K., Richard, P.G., 1980. Quantitative Seismology: Theory and Methods. Freeman, San Francisco.

Brekhovskikh, L.M., 1980. Waves in Layered Media, second ed. Academic Press, New-York.

Cagniard, L., 1962. Reflection and Refraction of Progressive Seismic Waves. Mc-Graw Hill, New York [Translation and revision by Flinn, E.A., Dix, C.H., of Cagniard, L., 1939. Réflexion et Réfraction des Ondes Séismiques Progressives. Gauthier-Villars, Paris.].

de Hoop, A.T., 1960. A modification of Cagniard's method for solving seismic pulse problems. Applied Scientific Research 8, 349–356.

de Hoop, A.T., van der Hijden, J.H.M.T., 1983. Generation of acoustic waves by an impulsive line source in a fluid/solid configuration with a plane boundary. Journal of the Acoustical Society of America 74 (1), 333–342.

Dieudonné, J., 1980. Calcul infinitésimal. Hermann, Paris.

Eringen, A.C., Suhubi, E.S., 1975. In: Elastodynamics, vol. II, Linear Theory. Academic Press, New York.

Fung, Y.C., 1990. Strength, Trauma and Tolerance. In: Biomechanics Motion, Flow, Stress, and Growth. Springer-Verlag, New-York.

Grimal, Q., Naïli, S., Watzky, A., 2002a. A study of transient elastic wave propagation in a bimaterial modeling the thorax. International Journal of Solids and Structures 39 (20), 5345–5369.

Grimal, Q., Naïli, S., Watzky, A., 2002b. Transient elastic wave propagation in a spherically symmetric bimaterial medium modeling the thorax. International Journal of Solids and Structures 39 (25), 6103–6120.

Grimal, Q., Watzky, A., Naïli, S., 2002c. A one-dimensional model for the propagation of pressure waves through the lung. Journal of Biomechanics 35, 1081–1089.

Issacson, E., Keller, H.B., 1966. Analysis of Numerical Methods. John Wiley and Sons.

LePage, W.R., 1961. Complex Variables and the Laplace Transform for Engineers. Dover Publications, New-York.

Pao, Y.H., Gajewski, R.R., 1977. The generalized ray theory and transient response of layered elastic solids. In: Mason, W.P. (Ed.), Physical Acoustics, vol. 13, pp. 184–265.

Shuvalov, A.L., Gorkunova, A.S., 1999. Cutting-off effect at reflection-transmission of acoustic waves in anisotropic media with sliding-contact interfaces. Wave Motion 30, 345–365.

Spencer, T.W., 1960. The method of generalized reflection and transmission coefficients. Geophysics 25, 625–641.

van der Hijden, J.H.M.T., 1987. Propagation of Transient Elastic Waves in Stratified Anisotropic Media. In: North Holland Series, Applied Mathematics and Mechanics, vol. 32.

Verweij, M.D., Chapman, C.H., 1997. Transmission and reflection of transient elastodynamic waves at a linear slip interface. Journal of the Acoustical Society of America 101 (5), 2473–2484.